Simulation of martensitic microstructural evolution in zirconium

U. Pinsook and G. J. Ackland
Department of Physics and Astronomy, The University of Edinburgh, Edinburgh, EH9 3JZ, Scotland, United Kingdom
(Received 4 March 1998)

A twinned microstructure is frequently observed after a martensitic phase transition. In this paper we investigate the atomic-level processes associated with the twin formation in a model system, using a many-body potential parametrized to represent zirconium. Molecular-dynamics simulations of the martensitic phase transition from bcc to hcp in zirconium show the evolution of a laminated twinned microstructure. Plastic deformation also occurs, creating basal stacking faults. The plastic deformation is such as to cause a rotation of the twins. This alters the twinning angle to the 61.5° angle of the low-energy $(10\bar{1}1)_{hcp}$ twins. These are thus identified as a cause of microscopic irreversibility in the transition. [S0163-1829(98)01534-3]

I. INTRODUCTION

A number of metals which have the body-centered-cubic (bcc) structure at high temperature exhibit a temperature-induced phase transition to a hexagonal-close-packed (hcp) phase at low temperature. This is a first-order martensitic transition, which proceeds via the Nishayama-Wassermann mechanism.[1] This is associated with the instability of a transverse N-point phonon in the bcc lattice and occurs when the temperature is lower than 1136 K. This phonon is stabilized by large anharmonic fluctuations at a higher temperature.[2,3]

In previous work, the development of martensitic microstructure during the transition has been investigated by a simplified model, using strain components as the order parameters.[4,5] In that model, anharmonic effects were included, but the existence of hcp variants was limited to two possible orientations. In practice, the symmetry of the phase transition allows for up to six equivalent hcp variants, all of which should be included for a realistic atomistic study.

Here we employ the molecular-dynamics approach in which atoms are treated individually, and so the appropriate symmetries of the transition are automatically included. Furthermore, the full anharmonicity can be included via the interatomic potential, as is the relative stability of the various crystalline phases, their point, line, and planar defects, and the anisotropic elasticity. To examine microstructure, large numbers of atoms are required because of the possible importance of long-range strain fields in nucleation. Thus the potential must have a functional form that is sufficiently fast to compute that large-scale calculations are feasible.

Obtaining a potential that satisfies all these criteria is not straightforward. For this reason previous simulational work at the atomistic level has been rather limited. Using static relaxation the energetics and relaxed structure of twins and twinning dislocations in the hcp phase have previously been studied,[6,7] as has the collapse of vacancy loops and generation of basal and prism stacking faults.[8] Anomalies in vacancy and self-diffusion migration have also been reported,[9] and these have been shown to be associated with the nonideal c/a ratio of zirconium.[10] The bcc phase itself has been characterized as being dynamically stabilized by phase fluctuations.[11]

In a previous molecular-dynamics (MD) study the evolution of the transition in a titanium-vanadium alloy has also been simulated at a low temperature,[12] but no twinned microstructure was observed. Likewise, the martensitic transition in iron has also been investigated using MD: this differs from zirconium in that it is between face centered cubic (fcc) and bcc rather than hcp and fcc. Again no microstructure was observed.

In our study, we use molecular dynamics to simulate the time evolution of martensite microstructure after rapid quenching from the bcc phase to 600 K. We show that for simulations above a certain size, a twinned microstructure is developed that has been suppressed by finite-size effects in previous studies. We report a number of features in the transition, including stress-induced nucleation and subsequent ripening of the microstructure. In principle, the transition mechanism is microscopically reversible, but we show that plastic deformation occurs, driven by the energy cost of forming the twin boundary; this is very sensitively dependent on the crystal geometry.

II. THE POTENTIAL

The series of molecular dynamics simulations reported here were done using the MOLDY code[13] with a 1-fs time step and up to 11 520 atoms. A many-body interatomic potential was used,[14,15] and since it will be shown that the results are closely related to other predictions of the potential, these will be reviewed briefly here.

The potential was fitted to the anisotropic elastic properties of the material, the nonideal c/a ratio (1.595), the cohesive energy of the hcp crystal structure relative to other possible structures,[16] and the energetics of vacancies and stacking faults. It has been shown to give a good description of other point-defect properties[16] and twin-boundary energies.[6] This is important since defects may be generated during the phase transition, and the scale of the energy minimizing microstructure is governed by the relative energies of twin boundaries and strain.[17,18]

The potential gives a good description of both bcc and hcp phases, with a phase transition from bcc to hcp occurring between 1330 and 1390 K (Ref. 19) depending on cooling rate and boundary conditions.

The energy is written in the form[20]

TABLE I. Parameters for potential function.

k	A_k (eV/Å^3)	R_k (Å)	a_k (eV^2/Å^3)	r_k (Å)
1	−0.61248219	5.5763004	0.50569395	5.5763004
2	0.87645549	5.4848856	−0.00890725	4.7992749
3	−0.21947820	5.2106413		
4	−0.01371379	4.3422011		
5	0.68830444	3.6565904		
6	1.45995293	3.1995166		

$$E_i=\frac{1}{2}\sum_j V(r_{ij})-\sqrt{\rho_i}, \tag{1}$$

where

$$V(r)=\sum_{k=1}^{6} A_k(R_k-r)^3H(R_k-r), \tag{2}$$

and

$$\rho_i=\sum_j \phi(r_{ij})=\sum_j \sum_{k=1}^{2} a_k(r_k-r_{ij})^3H(r_k-r_{ij}), \tag{3}$$

where $H(x)$ is the Heaviside step function, r_{ij} is the separation between atoms i and j, and the fitted parameters are given in Table I.

The potential does not model the rapid electronic heat conduction, so the temperature in the simulation is regulated with a Nose-Hoover thermostat to remove the latent heat released by the phase transition.

One other feature of the model is worthy of note: the primary dislocation slip system according to this model is basal slip, not prism slip as observed experimentally. This may be due to the low basal stacking fault energy, which allows basal dislocations to split into partials connected by a ribbon of stacking fault. Basal slip is common in hcp metals, but is believed to be a secondary slip mechanism in zirconium.[21]

III. TRANSITION MECHANISM

The conventional model for the transformation from bcc to hcp can be regarded as an orthorhombic distortion of the bcc lattice. An hcp variant requires a compression of 9.6% along one of $\langle 001\rangle_{bcc}$ direction and an extension of 10.9% in a corresponding $\langle 110\rangle_{bcc}$ direction to form a close-packed plane from a $(1\bar{1}0)_{bcc}$ plane. From various combinations of these directions, it can be seen that there are six possible hcp martensite variants, corresponding to different orientations of the c axis, into which bcc can transform.

The transformation is not purely defined by a strain of the unit cell, since a relaxation of the internal coordinates is also required, i.e., alternate $(1\bar{1}0)_{bcc}$ layers shuffle by 0.94 Å. This corresponds to a freezing in of the N-point phonon in the bcc lattice. If this shuffle does not occur cooperatively throughout the variant, stacking faults can be formed within a single variant. This is the Nishayama-Wassermann mechanism; the shuffle of successive layers distinguishes it from the Burgers mechanism that obtains the same orientation between bcc and hcp but in which the atoms move into these positions via a shear of successive layers. In a martensitic transition the Nishayama-Wassermann mechanism is preferred because it leads to less overall change of shape of the crystallite.

The maximum distance moved by individual atoms in this perfect transition path relative to their neighbors is 0.47 Å, so the mechanism is martensitic rather than diffusive. Curiously, the equivalent of the N-point phonon that would be involved in the reverse (hcp-bcc) transition is not a normal mode in the hcp lattice.[22] This may also explain the observation that the Burgers mechanism is responsible for the bcc to fcc transition in iron, while the Bain mechanism is followed in the reversed fcc to bcc.

The $\langle 111\rangle_{bcc}\rightarrow\langle 10\bar{1}0\rangle_{hcp}$ directions consist of a line of nearest neighbors in both structures, so there is very little strain in this direction during the transition. Moreover, for a given $\langle 10\bar{1}0\rangle_{hcp}$ direction, there are three hcp variants with close-packed planes containing this direction. Consequently, combinations of these three variants can be viewed in a planar slice perpendicular to this direction. For this reason, it is convenient to set an axis of the initial simulation cell along $\langle 111\rangle_{bcc}$.

IV. CALCULATIONS

We performed a number of simulations of 50-ps duration using a 1-fs time step and a fourth-order Gear predictor-corrector algorithm. The initial conditions comprise a homogeneous high-temperature bcc lattice a with the equilibrium value of the lattice parameter corresponding to the potential at 1400 K. Quenching to 800 or 600 K was done either by instantaneous rescaling of the temperature, or by use of the Nose-Hoover[23] thermostat. Boundary conditions were either constant volume or constant pressure in the Parrinello-Rahman[24] scheme. The qualitative results were independent of these parameters.

A range of unit-cell shapes and sizes were investigated. Two orientations were tried: the unit cell oriented along $(100)_{bcc}$, $(010)_{bcc}$, and $(001)_{bcc}$ or along $(1\bar{1}0)_{bcc}$, $(11\bar{2})_{bcc}$, and $(111)_{bcc}$. In both cases the transition was via the Nishiyama-Wassermann mechanism,[1] as described above.

Analysis of the simulation was performed every 5 ps as follows. The temperature was taken from the instantaneous kinetic energy via the standard relation $KE=1.5k_BT$ while the overall crystal structure was determined from the radial distribution function (Fig. 1 shows typical radial distribution functions for hcp and bcc).

The microstructure was examined by taking a snapshot from the MD simulation and then relaxing the atoms to their local minimum-energy configuration. From the relaxed structure, each atom was classified as hcp, bcc, or fcc according to its nearest-neighbor coordination shell, considering both symmetry and orientation. Assuming the Nishayama-Wassermann mechanism, there are six possible directions for the hcp c axis and these variants were identified separately. As described above, only three variants were ever observed in a single simulation. Some atoms, typically at twin boundaries, cannot be classified by this method and are labeled ''unknown.''

Once the atoms have been associated with a particular

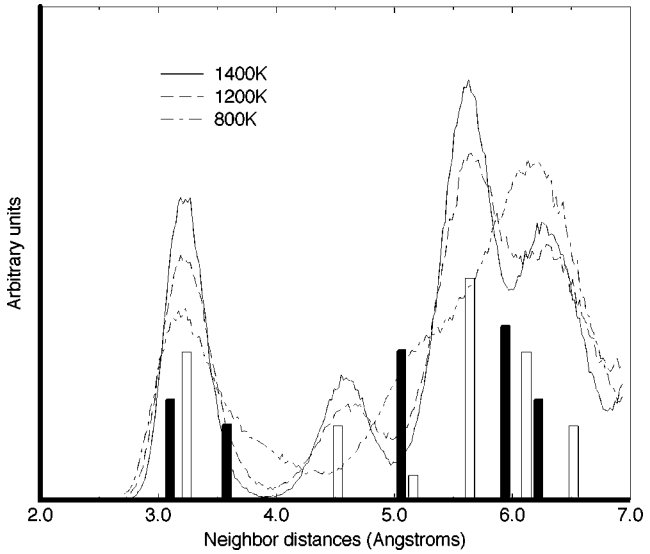

FIG. 1. The high-temperature phases are identified from their radial distribution function: the graph shows the characteristic hcp pattern at 800 and 1200 K, while at 1400 K the bcc pattern [broad first peak containing 14 (two shells) neighbors, absent second peak] is clearly different. The filled bars show the ideal peak positions for a bcc structure and the open bars those for hcp, while the bar heights are proportional to the number of atoms at that location. Quenching instantaneously to 0 K gives an hcp radial distribution function in each case.

structure, the $(111)_{bcc}$ direction which defined the plane of the microstructure was deduced. The different local coordinations were plotted in different colors, and slices through the sample perpendicular to the $(111)_{bcc}$ direction were examined visually to determine the microstructure.

A large number of simulations have been performed, with varying crystallographic orientation of the bcc lattice, and varying aspect ratio. A number of common features emerge, which we discuss generally, and then illustrate in the context of a single simulation.

V. STRESS-INDUCED PREFERENTIAL NUCLEATION AND METASTABLE PHASE FORMATION

Immediately on cooling, a region of hcp is nucleated. Because of the transition strain, this hcp region sets up a stress field around it in the plane of that strain $(111)_{bcc}$. This stress field can be accommodated by formation of the other two variants for which this particular $\langle 111\rangle_{bcc}$ lies in the close-packed plane. Thus two more variants are preferentially nucleated, and a columnar structure is established. Note that while the specifics of this nucleation depend on the transition mechanism, the preservation of lines of close-packed atoms (here $\langle 111\rangle_{bcc}$) is common to most martensitic transitions. Thus we believe that this is a general feature that will reduce the number of nucleated variants below that which is geometrically possible. Furthermore, because only a small amount of strain is required, the martensite can grow very quickly along the direction of the preserved close-packed line, defining the preferred plane for the martensite/parent interface.

As soon as the growing nuclei meet one another, a 60° rotation twin boundary is formed, the angle being that between, e.g., the $(101)_{bcc}$ and $(110)_{bcc}$ planes in the parent phase. This boundary may be either symmetric or asymmetric: If only two variants are present in a laminate microstructure, then all boundaries can be symmetric, but if finite regions of all three variants are present, some asymmetric boundaries must be formed. In the present case, the symmetric boundary has lower energy, and this provides a driving force for the elimination of one of the variants.

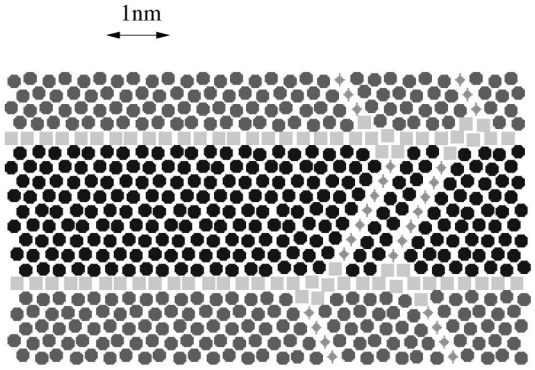

FIG. 2. A relaxed configuration indicating the structure of the twins. Darker circles represent the two hcp variants and stars are stacking faults that have local fcc coordination. Squares are boundary atoms that cannot be classified as hcp or fcc. The long straight sections have identical structure to the $(10\bar{1}1)_{hcp}$ twin boundaries calculated by Serra and Bacon (Ref. 6), while the stacking faults serve to rotate the twins towards 60°.

An interesting feature that occurs in the very early stages of microstructural evolution is the appearance of the fcc structure. This structure has a higher free energy than hcp, both according to the potential and in real zirconium. However, it is able to form a low-energy grain boundary with all three variants simultaneously. Thus it is found that for rapid cooling where the microstructure is very fine, small regions with the fcc structure appear. These regions may persist while all three variants still exist, but once the laminar microstructure is established, they are eliminated. It is worth noting, however, that in those regions that transform first to fcc and then to bcc, the ''memory'' of their original position in the bcc structure is lost. This may be a microscopic cause for the absence of the shape memory effect in zirconium (other sources of plastic deformation will be discussed later).

VI. STACKING FAULTS AND TWIN ROTATION

The relationship between the stacking faults and the transition is of interest, since stacking faults are metastable defects but do not anneal out in our calculations. In zirconium, we find that the tilt angle between two bcc-derived variants is 60°; this is very close to the 61.5° symmetric tilt boundary of $(10\bar{1}1)_{hcp}$ twins with low boundary energy that we calculate as $165.8\ \mathrm{mJ\,m^{-2}}$ according to this potential following the methods of Refs. 6 and 25. The twin boundary straightens toward $(10\bar{1}1)_{hcp}$.

There remains a discrepancy in angle that is made up by twinning dislocations; however, when the twins are small these may appear as partial twinning dislocations with a basal stacking fault extending through the twins (see Fig. 2). Close inspection shows that these stacking faults are not ar-

ranged at random, but rather an even number of layers apart leading to a systematic rotation of the variants toward the 61.5° angle that minimizes the boundary energy. To obtain that strain exactly would require one stacking fault every ten close-packed planes. Over a series of 30 calculations we have found an average of one stacking fault per 9.7 close-packed planes, in excellent agreement with the theoretical value. By motion of these stacking faults it would be possible for the crystal to deform plastically and the boundary to evolve to the stable $(10\bar{1}1)_{hcp}$ tilt without much diffusion of atoms from the parent bcc phase positions. However, although some mobility of the stacking faults is observed, it is too slow for this annealing process to occur on the time scale of our simulations.

VII. A TYPICAL SIMULATION

Having described the individual features of the transition microstructure, we now illustrate the entire process by following a single simulation.

The orientation of the bcc lattice with respect to the simulation cell is $x=[1\bar{1}0]_{bcc}$, $y=[11\bar{2}]_{bcc}$, and $z=[111]_{bcc}$. The dimensions of the cell are set to $x=101.50$ Å, $y=105.48$ Å, $z=24.86$ Å. To simulate the initial bcc phase and the final hcp phase in the same simulation, we use periodic boundary conditions and find that no remnant of the bcc phase persists at low temperature. After equilibration, the temperature is reduced to 600 K where the simulation is run and the evolution of the microstructure followed.

In our chosen simulation, the $\langle 111\rangle_{bcc}$ direction that transforms to $\langle 10\bar{1}0\rangle_{hcp}$ lies along the z axis of our simulation cell. This means that we can represent the microstructure by considering a single xy-plane slice, as in Fig. 3. The other such planes are similar.

Within the first 5 ps, Fig. 3(a), four strips of laminated 60° twins are formed. These twins correspond to two of the possible hcp variants. The twin boundary is close to the $(10\bar{1}1)_{hcp}$ plane. Referring to experimental and other computational results, $(10\bar{1}1)_{hcp}$ twins grow only under a highly stressed sample at high temperature.[6,7] Here, the 60° angle is forced by the relationship to the parent bcc phase. At this stage, some metastable structures including a number of stacking faults (which manifest themselves as diagonal lines of fcc-coordinated atoms) are produced, and a small region of rather random close packing is nucleated.

By 10 ps, the random close-packed region has ordered into a small lump of the third hcp variant.

During the period to 30 ps, the thinner of the strips of one hcp variant is gradually replaced by the other variant. This coarsening of the microstructure is analogous to Ostwald ripening, in which two twin boundaries are removed. The atoms in this region have now moved away from their previous sites in plastic deformation, and they have a different set of nearest neighbors.

After 40 ps, only three regions of three distinct variants are left. Two variants clearly dominate forming the familiar martensitic laminate microstructure. The final two figures show a small amount of further evolution as the boundaries straighten and sharpen.

The final picture is at 50 ps, the same as the previous, except that those atoms that have nearest neighbors other than the original 14 from the bcc structure are marked in white. This gives some indication of the amount of plastic deformation that has occurred, and hence of sources of irreversibility in the transition. Of course, the thickness of the laminate is now determined by the finite size of the simulation cell.

Although the chosen simulation shows most of the behavior observed in the other 20 simulations on similar cells, it is important to recognize that the nucleation is to some extent random. In some of the simulations the $\langle 111\rangle_{bcc} \rightarrow \langle 10\bar{1}0\rangle_{hcp}$ direction did not lie along the z axis. In others, only two strips of two variants were nucleated, and hence no coarsening was observed. The third variant did not appear in many of the simulations. This variety of behaviors gives us confidence that the nucleation phase is not dominated by finite-size or boundary-condition effects.

VIII. FINITE-SIZE EFFECTS

Previous atomistic-level molecular-dynamics work has not observed microstructure for the simple reason that the simulations are too small. The microstructure forms because the energy of forming twin boundaries is less than the strain energy of accommodating the hcp structure into the bcc cell.[26] Simple scaling laws show that for a simulation cell of length L, the energy associated with the twin boundary area grows as L^2, while the strain energy grows as L^3; consequently the microstructure becomes favored in a large system.

There are several similar finite-size considerations, and we explain here which features are affected by finite-size effects.

The appearance of regions of fcc is a finite-size effect, being due to a balance between high-energy asymmetric twin boundaries (L^2) and the energy difference between hcp and fcc (L^3). However, when the microstructure is very fine, in the early stages of growth, these fcc regions are genuinely stable. In the simulation they are eliminated not because of the scaling laws, but because the need for high-energy asymmetric twin boundaries in the microstructure is removed when the microstructure ripens to contain only two variants. In this sense, the temporary appearance of the fcc phase is expected to be a real phenomenon occurring early in the microstructural evolution, and not an artifact of the finite size of our system.

IX. CONCLUSIONS

A series of molecular-dynamics simulations that used a many-body potential have been carried out to describe the bcc-hcp transition in a model of zirconium. These calculations give insights into the atomic-level evolution of the microstructure during and shortly after the transition. By using a variety of simulation shapes and sizes, investigating both constant-volume and constant-pressure boundary conditions, and different quenching methods, we have demonstrated that the observed qualitative microstructural features are independent of the details of the simulation (except for finite-size effects).

A particular $\langle 111\rangle_{bcc}$ direction, apparently found randomly from the four possibilities, defines both the transfor-

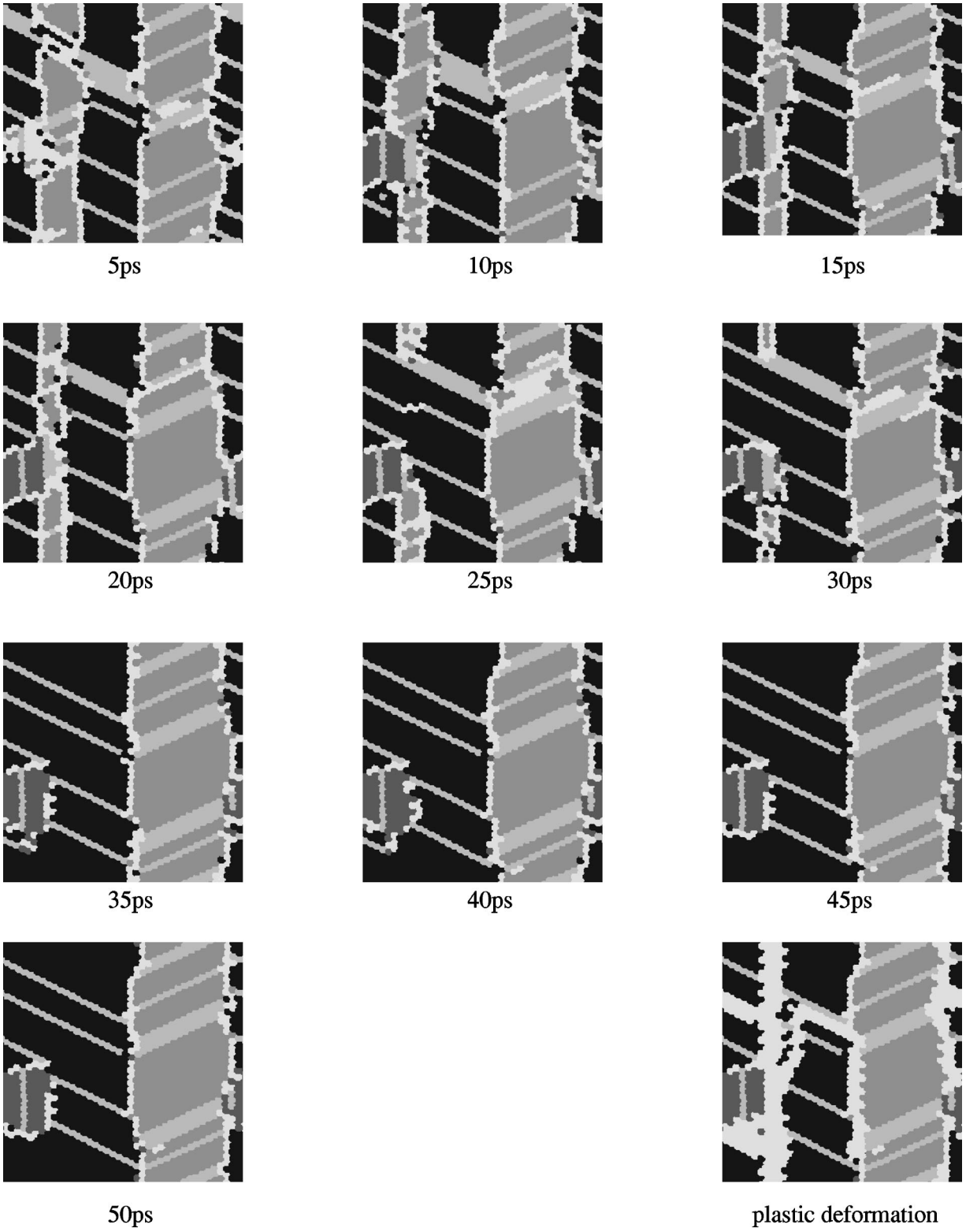

FIG. 3. Ten snapshots, taken at 5-ps intervals, of configurations quenched from the MD simulations. The black, dark gray, and mid-gray regions are hcp-coordinated variants, the light-gray regions are fcc (generally these are stacking faults) while the white are unclassifiable atoms (typically in the atomically sharp twin boundary). The final picture is from the same configuration as the tenth (50 ps), with atoms having different neighbors from their original bcc-coordination shell colored white. Further examples can be seen at http://www.ph.ed.ac.uk/may/works

mation plane (in practice, the interface between parent and martensite) and three possible hcp variants. The final microstructure involves twins comprising two variants of the hcp, i.e., $(10\bar{1}1)_{hcp}$ twins; this minimizes macroscopic strain of the crystal, and this is what is observed after some time. However, in the actual calculation we observe that a third variant is nucleated at the transition and subsequently destroyed. The microstructure also coarsens with time.

Some microscopically irreversible plastic deformation also occurs that is probably rapid motion of basal-plane partial dislocations leaving stacking faults as their signature. The driving force for this is the energy difference between the martensitic 60° incommensurate symmetric tilt twin boundaries and the 61.5° commensurate $(10\bar{1}1)_{hcp}$ twins. The effect of the dislocations is to rotate the twins, introducing microscopic irreversibility into the transformation.

This work introduces a criterion for microscopic irreversibility that may be of general relevance for creation of shape memory effect alloys, namely, the existence of metastable phases such as fcc, which may be stabilized by local strain or boundary energy considerations, and the existence of low-energy twin boundaries at angles close to, but not at, the angle dictated by the transition mechanism.

[1] Z. Nishiyama, *Martensitic Transformations* (Academic, New York, 1978).

[2] F. Willaime and C. Massobrio, Phys. Rev. B **43**, 11 653 (1991).

[3] Y.-Y. Ye, Y. Chen, K.-M. Ho, B.N. Harmon, and P.-A. Lindgård, Phys. Rev. Lett. **58**, 1769 (1987).

[4] P.-A. Lindgård and O.G. Mouritsen, Phys. Rev. Lett. **57**, 2458 (1986).

[5] T. Castán and P.-A. Lindgård, Phys. Rev. B **40**, 5069 (1989).

[6] A. Serra and D.J. Bacon, Mater. Sci. Forum **126-128**, 69 (1993).

[7] J.R. Morris, Y.-Y. Ye, K.-M. Ho, C.-T. Chan, and M.-H. Yoo, Philos. Mag. A **72**, 751 (1995).

[8] V.G. Kapinos, Y.N. Osetsky, and P.A. Platonov, J. Nucl. Mater. **195**, 83 (1992).

[9] A.G. Mikhin and Y.N. Osetsky, J. Phys.: Condens. Matter **5**, 9121 (1993).

[10] A.G. Mikhin, Y.N. Osetsky, and V.G. Kapinos, Philos. Mag. A **1**, 25 (1994).

[11] B.L. Zhang, C.Z. Wang, K.-M. Ho, D. Turner, and Y.-Y. Ye, Phys. Rev. Lett. **74**, 1375 (1995).

[12] P. Dang and M. Grujicic, Modell. Simul. Mater. Sci. Eng. **4**, 123 (1996).

[13] G.J. Ackland, Ph.D. thesis, Oxford University, 1987; M.W. Finnis, UKAEA Report No. AERE R13182, 1988 (unpublished).

[14] M.W. Finnis and J.F. Sinclair, Philos. Mag. A **50**, 45 (1984); **53**, 161 (1986).

[15] M.S. Daw and M.I. Baskes, Phys. Rev. B **29**, 6443 (1984).

[16] G.J. Ackland, S.J. Wooding, and D.J. Bacon, Philos. Mag. A **71**, 553 (1995).

[17] J.M. Ball and R.D. James, Z. Angew. Math. Mech. **76**, 389 (1996).

[18] J.M. Ball and R.D. James, Arch. Ration. Mech. Anal. **100**, 13 (1987).

[19] G.J. Ackland and U. Pinsook, in *Microscopic Simulation of Interfacial Phenomena in Solids and Liquids*, edited by S.R. Phillpot, P.D. Bristowe, D.G. Stroud, and J.R. Smith, MRS Symposia Proceedings No. 492 (Materials Research Society, Pittsburgh, 1998).

[20] G.J. Ackland, G.I. Tichy, V. Vitek, and M.W. Finnis, Philos. Mag. A **56**, 735 (1987).

[21] M.H. Yoo, Metall. Trans. A **12**, 409 (1981).

[22] J. Gavartin (private communication).

[23] S. Nose, J. Chem. Phys. **72**, 2384 (1984); W.G. Hoover, Phys. Rev. A **31**, 1695 (1985).

[24] M. Parrinello and A. Rahman, J. Appl. Phys. **52**, 7182 (1981).

[25] V. Vitek, G.J. Ackland, and J. Cserti, *Alloy Phase Stability and Design*, edited by G.M. Stocks, D.P. Pope, and A.F. Giamei, MRS Symposia Proceedings No. 186 (Materials Research Society, Pittsburgh, 1991), p. 237.

[26] We find that for any reasonable value of the fictitious box mass, the transition is too rapid for the Parrinello-Rahman MD box to change shape and thus accommodate the strain. This is consistent with the physical situation where the transition within a single grain is subject to the constraints imposed by surrounding grains.